molecular pharmaceutics

Article

Cite This: Mol. Pharmaceutics 2018, 15, 5427−5436

pubs.acs.org/molecularpharmaceutics

In Silico Discovery of a Small Molecule Suppressing Lung Carcinoma A549 Cells Proliferation and Inducing Autophagy via mTOR Pathway Inhibition

Jiyuan Liu,[†] Li Liu,[‡,§] Zhen Tian,[∥] Yifan Li,[†] Changhong Shi,[§] Junling Shi,[‡] Sanhua Wei,[⊥] Yong Zhao,[§] Caiqing Zhang,[§] Bing Bai,[§] Zhinan Chen,[*,#] and Hai Zhang[*,§,#]

[†]Key Laboratory of Plant Protection Resources & Pest Management of the Ministry of Education, College of Plant Protection, Northwest A&F University, Yangling, 712100 Shaanxi, China

[‡]Key Laboratory for Space Bioscience and Biotechnology, School of Life Sciences, Northwestern Polytechnical University, 127 Youyi West Road, Xi'an, Shaanxi Province 710072, China

[§]Laboratory Animal Center, Air Force Medical University, No. 169 Changle West Road, Xi'an, Shaanxi Province 710032, China

[∥]College of Horticulture and Plant Protection, Yangzhou University, Wenhui East Road, NO. 48, Yangzhou, Jiangsu Province 225009, China

[⊥]Department of Clinical Laboratory and Research Center, Tangdu Hospital, Air Force Medical University, No. 569 Xinsi Road, Xi'an, Shaanxi 710038, China

[#]National Translational Science Center for Molecular Medicine, Department of Cell Biology, School of Basic Medicine, Air Force Medical University, Xi'an, Shaanxi Province 710032, China

Supporting Information

ABSTRACT: Mammalian target of rapamycin (mTOR) kinase is vital to the regulation of cell growth and proliferation, and it has been taken as a promising target to develop cancer therapies. By reference to the crystal structure of mTOR−PP242, we explored to discover potential ATP-competitive inhibitors of mTOR. Through the integrated use of multiple in silico screenings, the tremendous amount of compounds from the SPECS database were finally reduced to 30. After several rounds of convincing biological tests in A549 cells, the newfound C-4 was identified as a potential ATP-competitive inhibitor of mTOR. Besides A549 cell proliferation suppression caused by C-4, autophagy was also determined through autophagosome observation and autophagy flux detection in C-4 treated A549 cells. We demonstrated that C-4 could inhibit cell growth and proliferation, and this inhibition may be associated with autophagy.

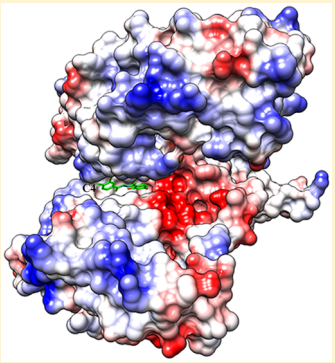

KEYWORDS: *pharmacophore modeling, virtual screening, mTOR kinase, inhibitor, autophagy*

INTRODUCTION

mTOR (mammalian target of rapamycin) pathway functions to regulate translation, metabolism, and transcription in response to nutrients and growth factors.[1−3] Central to the pathway is mTOR, a serine/threonine protein kinase belonging to the phosphatidylinositol kinase-related kinase (PIKK) family.[4,5] Through sensing and integrating extracellular and intracellular signals, the two structurally and functionally distinct mTOR complexes, termed mTOR complex 1 (mTORC1, also known as mTOR−Raptor complex) and mTORC2 (mTOR−Rictor complex), couple energy and nutrient abundance to the execution of cell growth and division.[6,7] As such, mTOR is often implicated in disease states, particularly cancers, where growth is deregulated and homeostasis is compromised. Not only that, mTOR also negatively modulates autophagy, a conserved cellular process tightly coupled to the regulation of cell growth.[6,8] Related researches reveal that inhibiting any mTOR-containing complexes is sufficient to induce autophagy.[9−12] For example, treatment of rapamycin (mTOR inhibitor) enhances the activity of ULK1 (UNC-51-like kinase 1), initiating autophagy in different types of cancer.[12] Meanwhile, autophagy can be induced in skeletal muscle and breast cancer cells by inhibiting mTORC2 under starvation condition.[10,11] Actually, mTOR deregulation is increasingly emerging as a modulator of cancer onset and progression.[13] The broad cellular functions of mTOR makes the protein kinase an attractive target for developing cancer therapies.[12,14,15]

Considerable enthusiasm has emerged in developing new mTOR inhibitors. Of the multiple methods applied, in silico

Received: September 21, 2018
Accepted: October 12, 2018
Published: October 12, 2018

DOI: 10.1021/acs.molpharmaceut.8b00996
Mol. Pharmaceutics 2018, 15, 5427−5436

drug discovery is the most prominent approaches currently used to search for inhibitor candidates of mTOR on a large scale.[15,16] Several mTOR inhibitors being evaluated in preclinical and clinical trials contain rapalogues (rapamycin and its analogues) and ATP analogues (ATP-competitive inhibitors).[17,18] As a representative ATP analogue, PP242 inhibits cell proliferation more completely due to the sustained and specific inhibition of mTOR in both mTORC1 and mTORC2.[8,15,18] To achieve the goal of identifying novel mTOR pathway inhibitors with PP242 being the prototype, the SPECS database is initially queried by a pharmacophore model derived from the cocrystal structure of the mTOR−PP242 complex (PDB ID: 4JT5).[5] After several rounds of in silico screening (Figure S1) and biological validation, small molecules suppressing cell proliferation via inhibiting the mTOR pathway were considered as target inhibitors.

EXPERIMENTAL SECTION

Molecular Dynamic Simulations. In the present research, the cocrystal structure of the complex formed by mTORdeltaN-mLST8 and PP242 (PDB ID: 4JT5, Chain A) was used as the initial structure for molecular dynamic (MD) simulations.[5] However, in the crystal structure 4JT5, the kinase domain (residues K1867-T2436) where PP242 binds was intact, while some loop domains (residues K1814-K1867 and T2436-A2492) were missing. What's more, no template was available to repair the missing loop domains. As a result, to eliminate the effects resulted from missing loop domains, the mTOR kinase domain was encapsulated by adding acetyl (ACE) to the K1867 residue on the N-terminus and *N*-methylamino (NME) to T2436 on the C-terminus.[19] Such optimization helps to guarantee the stability of the mTOR−PP242 complex in the following MD simulations. Since only the kinase domain was used in the MD simulations, the starting residue in our constructed structure corresponded to the 1866th residue in 4JT5. Thereafter, 100 ns MD analysis of the encapsulated mTOR−PP242 complex was performed using the Amber12 package.[20,21]

To perform MD simulations, parameters and charges of ligand PP242 were set by using GAFF and AMI-BCC methods,[22,23] protein parameters were depicted through a bioorganic system force field (ff9SB) from the Amber software.[24] As for the energy minimization of the mTOR−PP242 complex, it was performed by the steepest descent method for the first 5000 steps and the conjugate gradient method for the subsequent 5000 steps to eliminate unfavorable contacts. The solvated complex was equilibrated by the program composed of heating in the *NVT* ensemble from 0 to 300 K in 500 ps, density equilibration for 500 ps with weak restraints, and constant pressure with unrestrained equilibration at 300 K for 5 ns. To prevent the abrupt jump in the potential energy, the production phase was run for 100 ns using the same conditions as the equilibration phase. The coordinates were recorded every 10 ps, ensuring that the structures were uncorrelated sufficiently. All equilibration and production phase MD simulations were performed in the isothermal isobaric (*NPT*) ensemble using a Berendsen barostat.[25] For other details of MD simulations, please refer to our former reports.[19,20,26,27]

On the basis of the MD representative structure of mTOR−PP242, the mmpbsa.py module in Amber12 was used to quantify the interactions between PP242 and key residues of mTOR.[26,28] Per-residue energy decomposition was carried out based on the MM-PBSA method (molecular mechanics Poisson−Boltzmann surface area).[29−31] To provide guidance for further pharmacophore construction and modification, the MD trajectories of mTOR−PP242 were clustered using an average-linkage algorithm, and then residues contributing a total energy above 1.00 kcal/mol were analyzed by ASM (alanine scanning mutagenesis).[19,26,32]

Construction of Chemical Library for Virtual Screening. The chemical library for virtual screening was generated on the basis of the chemical structures of 210 265 compounds from the SPECS database (version Jun2015_10mg, www.specs.net). Using the OMEGA module and LigandScout software in combination,[33] 100 active conformations for each compound were generated to reproduce the flexibility of a molecule. After considering medicine principles and pharmaceutical properties comprehensively, 210 211 small molecules were finally kept to constitute the chemical library for prospective high-throughput virtual screening.

Pharmacophore Modeling. In the research, construction and refinement of the pharmacophore model were performed using LigandScout software.[21,27,33] Taking the results of conformation cluster analysis and per-residue energy decomposition as a whole, the structure-based pharmacophore was derived from the MD representative structure of the mTOR−PP242 complex.[34]

Multistep Virtual Screening. The flowchart for the multistep virtual screening used in the research is listed in Figure S1. By using the Iscreen module of LigandScout software, the final pharmacophore model was applied to query the constructed chemical library. Only those matching all query features were considered as hits. Hits were ranked according to their Pharmacophore-Fit Scores. To increase the accuracy of prediction, the Gaussian shape similarity and binding affinity calculations were applied successively. Molecules with a Gaussian shape similarity score no less than 0.50 were subjected to binding affinity calculations. Only those coupled with a binding affinity score less than −20 kcal/mol were kept for further filtration.[21,35]

An XED (extended electron distribution) molecular mechanics force field was applied as the final gatekeeper of virtual screening. To acquire the XED force field template of PP242, the FieldTemplater module of the Forge software (Cresset) was used to analyze the molecule shape, static electricity, and hydrophobic features of PP242 derived from the mTOR−PP242 complex.[36] After comparing the XED field template of PP242 and the hit compounds obtained earlier, those possessing the top 30 field similarity scores were purchased and used for biological tests.

Inhibition Tests in A549 Cells. Western blot analysis was used to test inhibitory effects of the 30 selected compounds against mTOR in the cell model. A549 cells were incubated with various concentrations of compounds for 24 h. After being washed with PBS (10 mM, pH7.4) 3 times, the collected cells were lysed with RIPA lysis buffer to extract protein. Proteins were separated with SDS-PAGE and transferred to a PVDF membrane. Thereafter, the membrane was washed with a PBST buffer, blocked with 5% skim milk, and incubated overnight at 4 °C with primary antibodies (anti-mTOR/-AKT/-p-mTOR/-p-AKT/-p-p70S6K1/-p-4EBP1/-actin). After being washed, the membrane was incubated with secondary antibodies for 1 h. Protein bands were visualized using ECL and quantified with ImageJ software (version 1.38).

DOI: 10.1021/acs.molpharmaceut.8b00996
Mol. Pharmaceutics 2018, 15, 5427−5436

Absolute Binding Free Energy Calculation. To compare the binding affinity of PP242 and C-4 to the mTOR kinase domain, the Waterswap absolute binding free energy method (abbreviated as Waterswap) from the Cresset Flare V2 software was applied. As an absolute binding free energy method, Waterswap worked by swapping the ligand bound to the protein with an equivalent shape and volume of water. The superimposed conformation of PP242 and C-4 obtained using the Forge software was taken as initial conformation for Waterswap. The absolute binding free energy for the target ligand was calculated by three different methods, namely, Bennett, TI, and FEP. A consensus for the binding free energy was further obtained by a weighted arithmetic mean of Bennett (50%), TI (30%), and FEP (20%) free energy estimators. By using very strict Monte Carlo (MC) sampling, the Waterswap absolute binding free energy method was verified to be highly reliable in former reports, and its calculated results were in good linear relation with the experimental results.[37−39]

To further approve the results of ASM, residue-based decomposition of the Waterswap absolute binding free energy for PP242 in the mTOR kinase domain was performed as well.[38]

Effects on Cell Proliferation. The compound exhibiting inhibitory effects on the mTOR kinase (C-4) was subjected to cell proliferation tests. A549 cells at the logarithmic phase were seeded into 96-well plates (5×10^3 cells/well) and incubated with various concentrations of C-4 for 48 h. Thereafter, CCK-8 (10 μL/well) was added and incubated for 3 h. The OD values of each well were measured under 450 nm with a spectrophotometer (Biotek). Treated cells were collected and stained with PI to determine cell cycle distribution. Finally, treated cells were also subjected to inverted microscopy to observe cell death status.

Autophagy Determination. The compound exhibiting inhibitory effects on the mTOR kinase (C-4) was chosen to observe its activity to induce autophagy in A549 cells. For detail, A549 cells were treated with 3.6 μg/mL C-4 for 24 h and collected. Cells were fixed overnight with 2.5% glutaraldehyde and treated with 0.1% osmium tetroxide for 1 h at 4 °C successively. After being dehydrated with graded acetone, cells were embedded in an epoxy resin and sectioned. The ultrathin sections were loaded onto a transmission electronic microscope (TEM, JEM-1230) to observe autophagosome morphology.

A549 cells at the logarithmic phase were seeded in 6-well plates and transfected with GFP-LC3 plasmids according to the manufacturer protocol. After 24 h, the transfected cells were treated with 3.6 μg/mL C-4 for 24 h. Then, the treated cells were fixed with 4% paraformaldehyde and permeabilized with 1% Triton X-100. After that, cells were stained with a primary antibody (anti-LC3) and secondary antibody (FITC-labeled goat anti-rabbit), and then the cells were stained with 1:10000 DAPI to visualize nuclei morphology. Samples were subjected to confocal laser scanning microscopy to observe the formation of autophagic puncta.

Western blot analysis was applied to check the changes of autophagic flux on titration of C-4. In the process, antibodies of LC3, P62/SQSTM1, Beclin1, and ULK1 were used. For detail, please refer to the Inhibition Tests in A549 Cells section.

Chemical Reagents and Antibodies. All of the tested compounds were purchased from Selleckchem (Huston, TX) and dissolved in DMSO for stock (50 mg/mL). For each experiment, the stock solutions were diluted to a set of concentrations by cell medium. Antibodies required in the research were provided by Abcam (Cambridge, MA) and used in 1:1000. The CCK-8 kit was purchased from 7sea Biotech (Shanghai, China).

Cell Culture. A549 cells were purchased from Type Culture Collection of the Chinese Academy of Sciences (Shanghai, China). In the present research, all cells were cultured in RPMI1640 plus 10% fetal bovine serum (FBS) under the humidified conditions of 37 °C, 5% CO_2.

Statistical Analysis. The cell inhibition rate (IR) was calculated using eq 1

$$\mathrm{IR} = \frac{\mathrm{OD}_{\mathrm{experiment}} - \mathrm{OD}_{\mathrm{control}}}{\mathrm{OD}_{\mathrm{control}} - \mathrm{OD}_{\mathrm{blank}}} \times 100\% \quad (1)$$

In the equation, $\mathrm{OD}_{\mathrm{experiment}}$, $\mathrm{OD}_{\mathrm{control}}$, and $\mathrm{OD}_{\mathrm{blank}}$ represent the corresponding OD values of treated groups, control groups, and blank.

Data are presented as the mean ± SD. A student's *t* test and one-way ANOVA were used to assess significant differences among experimental groups using SPSS software, version 12 (SPSS, Chicago IL). *p*-values < 0.05 or < 0.01 were considered statistically significant.

RESULTS AND DISCUSSION

Key Interactions between mTOR and PP242. Before constructing the pharmacophore model for prospective virtual screening, it is necessary to identify the key interactions between mTOR and PP242. We start by analyzing the crystal structure of the mTOR−PP242 complex (PDB ID: 4JT5) with a 100 ns MD simulation. As shown in Figure S2A, the mTOR−PP242 complex achieves equilibrium at about 25 ns with an averaged RMSD value of 3.12 ± 0.33 Å. For the ligand PP242, it reaches equilibrium earlier than the mTOR−PP242 complex with an RMSD fluctuating around 1.47 Å (SD = 0.15 Å) after the time point of 10 ns (Figure S2B). Such high stability guarantees the subsequent performance of per-residue energy decomposition and ASM.

Energy spectra of the mTOR−PP242 interaction are present in Figure 1A. Of the residues contributing more than 1.00 kcal/mol energy, eight (Leu320, Tyr360, Ile372, Gly373, Trp374, Val375, Met480, and Ile491) are positive to mTOR−PP242 binding (favorable residues), whereas three (Lys322, Asp330, and Asp492) are negative (unfavorable residues). To predict which favorable residues are hot spots, ASM is performed. Anyway, the energy contribution of Val375 mainly derives from its backbone (Table S1), and the MMPBSA.py module we used currently does not support the mutation of Gly to Ala. As a result, only the rest of the six favorable residues were subjected to ASM. According to the standards of hot-spot, warm-spot, and null-spot,[26] Tyr360 ($\Delta\Delta G_{\mathrm{bind}}$ = 4.29 kcal/mol) and Trp374 ($\Delta\Delta G_{\mathrm{bind}}$ = 4.17 kcal/mol) are categorized into hot-spot; Leu320 ($\Delta\Delta G_{\mathrm{bind}}$ = 2.51 kcal/mol), Ile372 ($\Delta\Delta G_{\mathrm{bind}}$ = 3.78 kcal/mol), and Ile491 ($\Delta\Delta G_{\mathrm{bind}}$ = 3.80 kcal/mol) are warm-spot; and Met480 ($\Delta\Delta G_{\mathrm{bind}}$ = 1.59 kcal/mol) is null-spot (Table 1). Residues of hot-spot are usually regarded as key residues involved in the interaction between mTOR and PP242.[32,40]

To confirm whether the results of MD-based free energy decomposition and ASM are dependable, the Waterswap binding free energy for PP242 in the mTOR kinase domain is

DOI: 10.1021/acs.molpharmaceut.8b00996
Mol. Pharmaceutics 2018, 15, 5427−5436

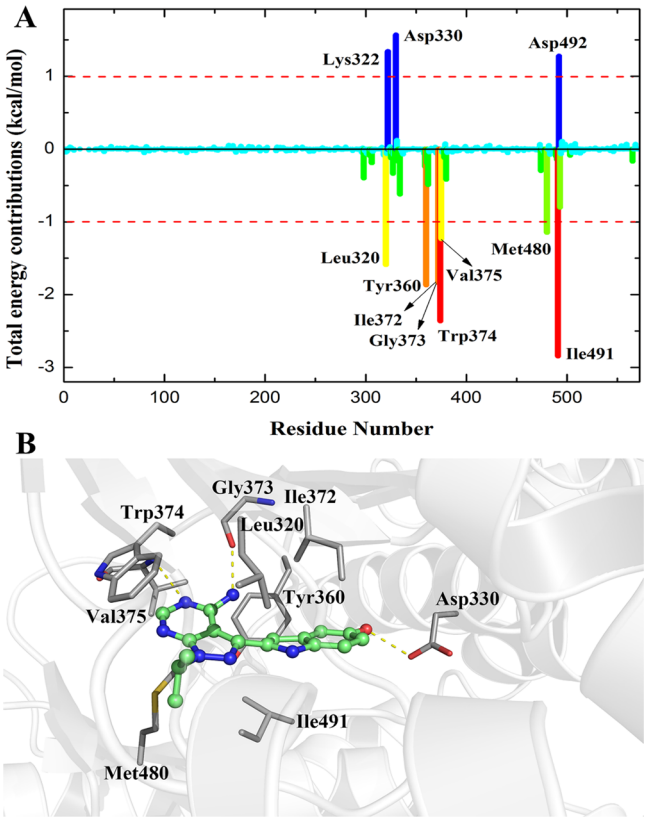

Figure 1. (A) Residue−ligand interaction spectra of the mTOR−PP242 complex. The *x*-axis denotes the residue number of the mTOR kinase domain, and the *y*-axis denotes the total energy contribution of each residue. (B) Key interactions at the active site observed during MD simulations of PP242. PP242 was present with the stick-and-sphere model. Color code: green, C; red, O; and white, H. Key residues are presented with stick model. Color code: gray, C; red, O; blue, N; white, H; and yellow-dashed line, H bond.

Table 1. Theoretical $\Delta\Delta G_{bind}$[a] Values for Wild-type and Mutant mTOR−PP242 Complexes

protein[b]	L320A	Y360A	I372A	W374A	M480A	I491A
$\Delta\Delta G_{bind\text{-}cal}$	2.51	4.29	3.78	4.17	1.59	3.80

[a]All values are given in kcal/mol. [b]L320A, Y360A, I372A, W374A, M480A, and I491A are the abbreviations for mTORL320A, mTORY360A, mTORI372A, mTORW374A, mTORM480A, and mTORI491A, respectively.

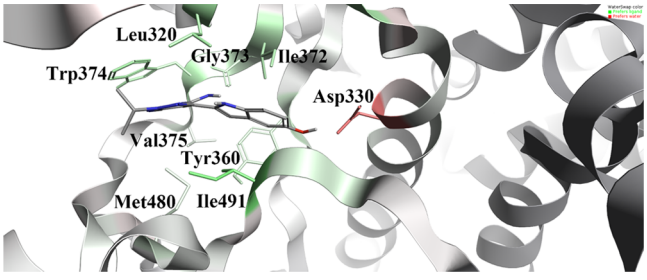

Figure 2. Residue-based decomposition of the Waterswap binding free energy for PP242 in the mTOR kinase domain. Residues favorable to the mTOR−PP242 interaction are shown in green, the darker the green is, the more favorable the residue is Residues unfavorable to mTOR−PP242 binding are shown in red.

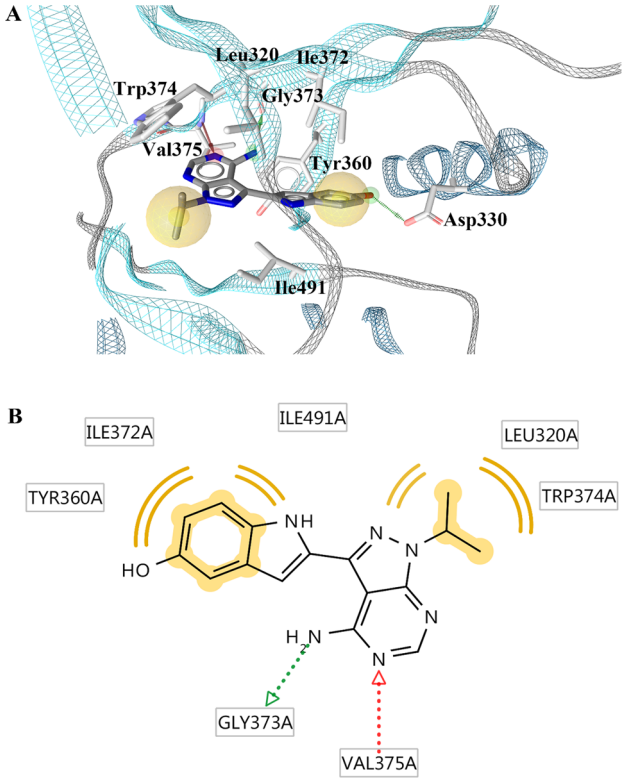

Figure 3. (A) The final pharmacophore model for prospective virtual screening. (B) The 2D interactions diagram of mTOR−PP242. In (A), the model consists of two hydrophobic features (yellow), two hydrogen bond features (hydrogen bond acceptor and hydrogen bond donor) (red and green arrow), and one optional hydrogen bond donor feature (green dash arrow). In (B), the 2D interaction diagram of PP242 with mTOR were visualized with the following color code: hydrogen bond acceptor (red arrow), hydrogen bond donor (green arrow), and hydrophobic interaction (yellow sphere).

further subjected to residue-based energy decomposition. In Figure 2, residues shown in green sticks represent those favorable to the mTOR−PP242 binding, with green color depth in positive correlation with residue contribution to the mTOR−PP242 interaction. Similar to ASM and MD, Tyr360, Trp374, Leu320, Ile372, Ile491, and Met480 are determined to be residues providing top contributions in Waterswap-based free energy decomposition as well (Figure 2, Table 1). Besides, the unfavorable residue ASP330 revealed by MD is also categorized into a negative one in the Waterswap method (Figure 2, Table S1).

Pharmacophore Modeling and Modification. The pharmacophore prototype is generated on the basis of the MD representative structure of the mTOR−PP242 complex (Figure 1B). As shown in Figure S3, the prototype is composed of three hydrophobic features, two H-bond donor features (HBD) and one H-bond acceptor feature (HBA). Specifically, the three hydrophobic features are formed between Tyr360/I491/Ile372 and the benzene group (PP242), Met480 and the pyrrole group (PP242), and Leu320/Trp374 and the isopropyl group (PP242), respectively. The HBA feature is formed between Val375 and the N atom of the PP242 pyrimidine group, whereas the two HBD features are detected between Asp330 and PP242 hydroxy, and Gly373 and PP242 amine (Figure S3).

DOI: 10.1021/acs.molpharmaceut.8b00996
Mol. Pharmaceutics 2018, 15, 5427−5436

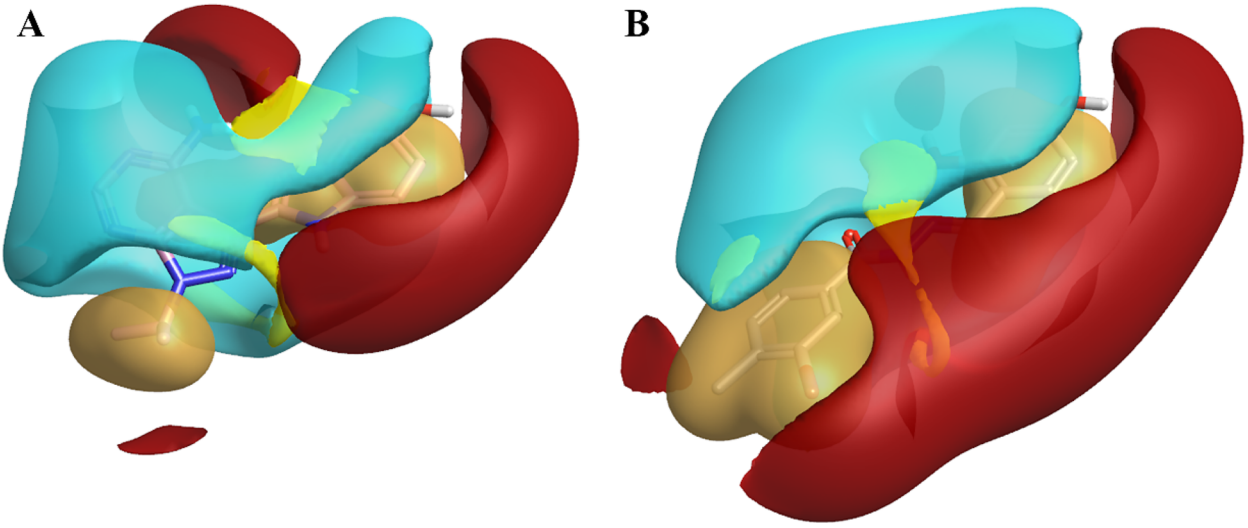

Figure 4. Average field representation of PP242 (A) and C-4 (B) in the mTOR kinase domain. Red and blue field surface highlight energy minima for positively and negatively charged probes, respectively. The yellow surface represents attractive van der Waals minima for neutral probes, and the gold surface represents hydrophobic centroids. PP242 and C-4 are present in the stick model with a pink and gray color, respectively.

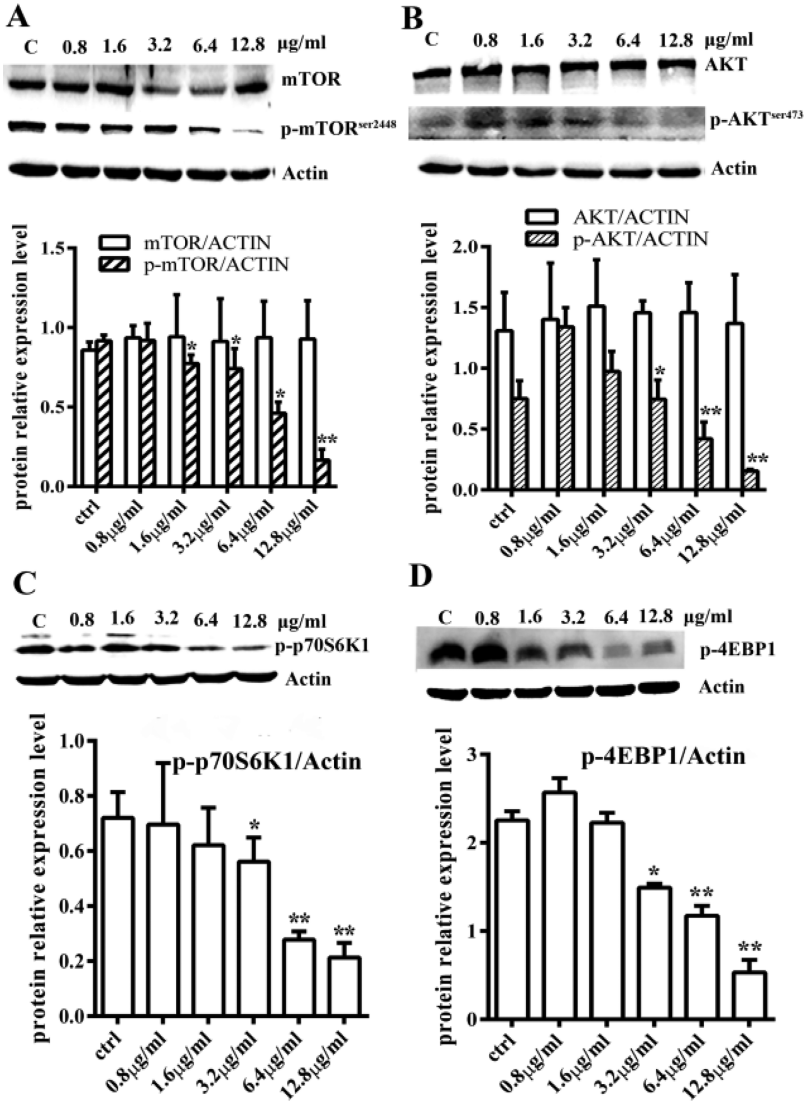

Figure 5. Inhibitory effects of C-4 on the mTOR kinase. The effects of C-4 on inhibiting mTOR (A), AKT (B), p70S6K1 (C), and 4EBP1 (D) phosphorylation.

DOI: 10.1021/acs.molpharmaceut.8b00996
Mol. Pharmaceutics 2018, 15, 5427−5436

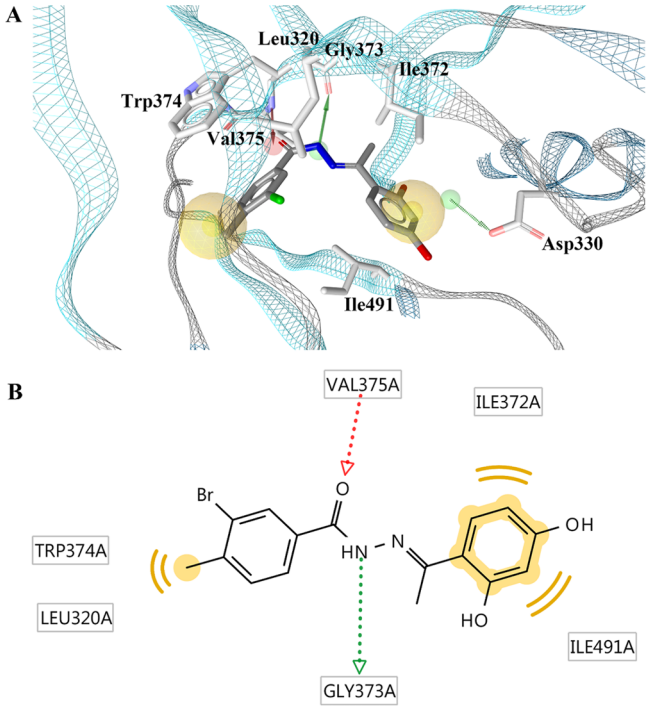

Figure 6. (A) The pharmacophore model derived from the mTOR–C-4 complex. The model consists of two hydrophobic features (yellow), one HBA feature (red arrow), one HBD feature (green arrow), and one optional HBD feature (green dash arrow). (B) The 2D diagram of mTOR–C-4 interaction. Red arrow, HBA feature; green arrow, HBD feature; and yellow sphere, hydrophobic feature.

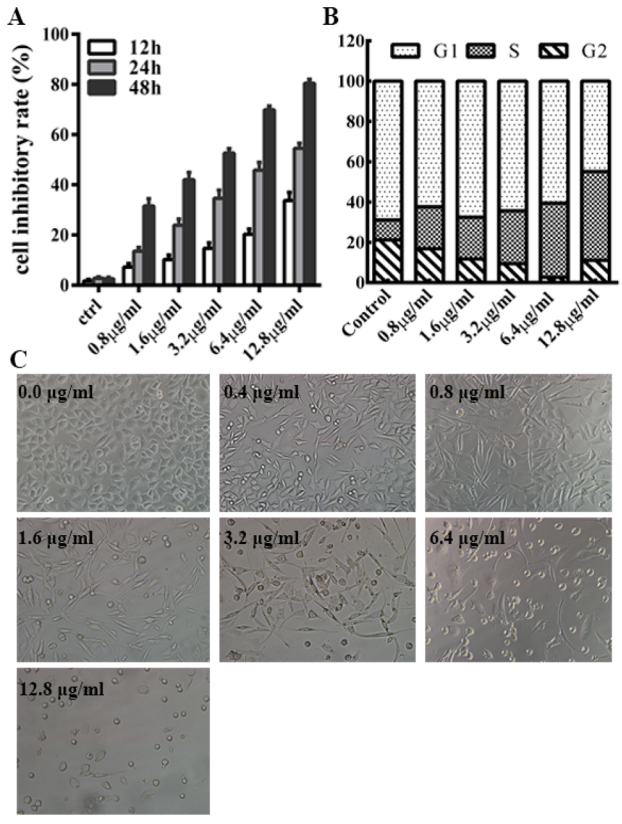

Figure 7. Cytotoxicity of C-4 on A549 cells. The effects of C-4 on inhibiting cell proliferation (A), blocking cell cycle (B), and inducing cell death (C).

To get the reliable pharmacophore model for prospective virtual screening, the prototype is refined on the basis of the results of energy decomposition (Table S1) and ASM (Table 1). The HBA and HBD features involved with Val375 and Gly373 are kept due to their remarkable contributions of static electricity energy (−1.64 and −2.36 kcal/mol, respectively) and rare unfavorable polar solvation energy (EPB) (Table S1). As a result of high unfavorable EPB (8.63 kcal/mol), Asp330 is unfavorable to the binding of PP242, even though its static electricity energy is as high as −7.66 kcal/mol. So the HBA feature between Asp330 and PP242 is set as an optional feature. Then, the hydrophobic feature between Met480 and the pyrrole group of PP242 is wiped off due to its null-spot role in the mTOR–PP242 interaction (Table 1). The rest of the two hydrophobic features involved with the hot-spot and warm spot are kept. As a whole, the final pharmacophore model for prospective virtual screening is refined to two hydrophobic features, one HBA feature, one HBD feature, and one optional HBD feature (Figure 3 and the Supporting Information).

Multi-Step Virtual Screening. Using the LigandScout fast flexible search algorithm, the SPECS screening library (~210 211 compounds) is initially queried by the optimized pharmacophore model. The 8094 compounds fully matching the final pharmacophore features are reserved as hits. Subsequently, the integrated application of the Gaussian shape similarity score and binding affinity score in LigandScout cut the number of hits to 929, with a binding affinity cutoff of −20.00 kcal/mol (Table S2). Considering the high accuracy and efficiency, an XED molecular mechanics force field is used as the final gatekeeper for the in silico discovery of target molecules. After comparing with the PP242 force field template (Figure 4A) (composing of molecular shape, static electricity, and hydrophobic features) generated on the basis of the mTOR–PP242 interaction, 30 compounds (Table S3) possessing top field similarity with that of PP242 were finally kept as potential inhibitors of mTOR and purchased from Selleckchem (Houston, TX) for subsequent biological tests.

C-4 Inhibits mTOR Pathway. As indicated by Western blot analysis, all selected compounds but C-4 exhibit little inhibitory effects against mTOR in A549 cells. As shown, the addition of C-4 (0–12.8 μg/mL) directly decreases the level of activated mTOR (p-mTOR^{ser2448}), which is phosphorylated at Ser2448 (Figure 5A). Not only that, the phosphorylation of downstream substrates of mTORC1 (p70S6K1 and 4EBP1) and mTORC2 (AKT) are all negative to the titration of C-4 (Figure 5B,C,D).

The Waterswap method was performed to evaluate the binding affinity between mTOR and C-4. By using highly strict MC sampling, the calculated results of Waterswap were proven to be in a good linear relation with the experimental results, and it was regarded as a comparatively new and fairly reliable method to identify protein–ligand affinity.[37−39] As shown in Table S4, the binding free energies of PP242 and C-4 obtained through the Waterswap method are −28.85 ± 1.3 and −22.96 ± 1.4 kcal/mol, respectively. Although the binding free energy of C-4 is not as good as that of PP242, C-4 does exhibit the binding affinity to the kinase domain of mTOR.

As mentioned above, the level of activated mTOR, as well as the phosphorylation of the mTOR downstream substrates (p70S6K1, 4EBP1, and AKT), all suffer from significant decreases in C-4-treated A549 cells (Figure 5). Considering the theoretical binding affinity between C-4 and mTOR, it can be concluded that C-4 is an mTOR inhibitor, and it acts to

DOI: 10.1021/acs.molpharmaceut.8b00996
Mol. Pharmaceutics 2018, 15, 5427−5436

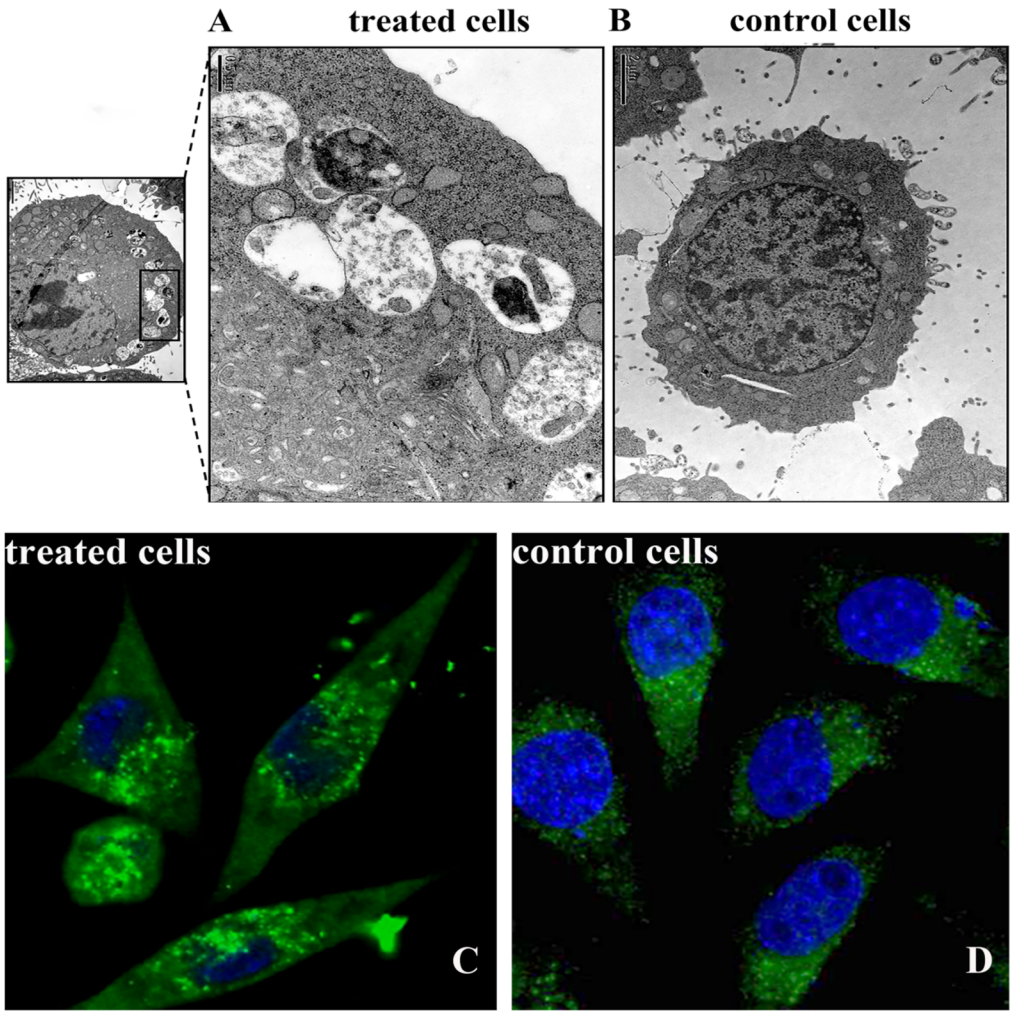

Figure 8. (A) The detection of autophagosomes by TEM in A549 cells treated with 3.6 (A) and 0.0 μg/mL (B) for 24 h. (B) The confocal immunofluorescence analysis of autophagic puncta in A549 cells treated with 3.6 (A) and 0.0 μg/mL (B) for 24 h.

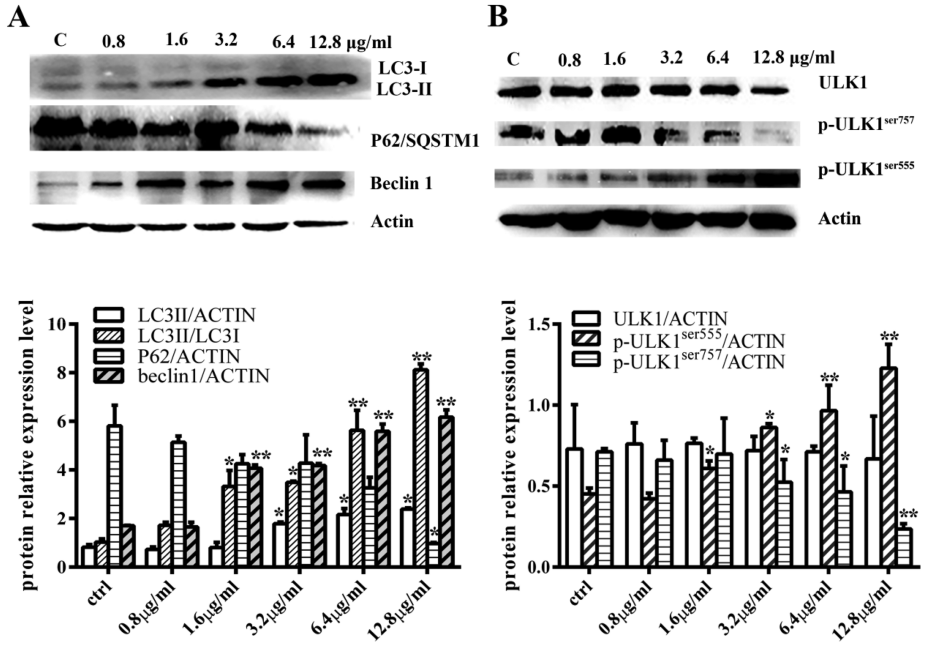

Figure 9. Autophagy flux measurement through Western blot analysis. On the titration of C-4, the relative expression level of key elements in the autophagy flux, including LC3-I, LC3-II, P62/SQSTM1, Beclin1, and phosphorylation of ULK1, exhibited corresponding changes.

DOI: 10.1021/acs.molpharmaceut.8b00996
Mol. Pharmaceutics 2018, 15, 5427−5436

block the mTOR pathway by probably inhibiting the activity of any mTOR-containing complexes.[7,17,18,41] What's more, the complete and comprehensive inhibition of mTOR leads to the supposition that C-4 may work similar to the prototyping molecule PP242 used for pharmacophore modeling.[8]

To determine the supposition, the pharmacophore model and XED mechanics force field of C-4 are further subjected to one-to-one matching with counterparts of PP242. The pharmacophore model derived from the mTOR−C-4 complex is presented in Figure 6. The acylhydrazides group of C-4 forms one HBA feature with Val375 and one HBD feature with Gly373, two hydrophobic features are detected between Trp374/Leu320 and the methyl of toluene (C-4) and Ile372/Ile491 and the benzene ring of resorcin (C-4), suggesting satisfactory pharmacophore matching with that of PP242 (Figures 3 and 6). Not only that, the XED fields of C-4 and PP242 are also similar to each other (Figure 4). According to the results listed in Table S3, the XED field similarity can reach as high as 60%.

Consequently, the high matching of the corresponding pharmacophores and XED fields derived from the mTOR−PP242 and mTOR−C-4 complexes validates that C-4 can be taken as a potential ATP-competitive mTOR inhibitor.[5,17,18] As expected, such inhibitors block the binding of ATP, which donates the phosphate group by which mTOR phosphorylates its target proteins, leading to the inhibition of any mTOR-containing complexes (mTORC1 and mTORC2).

C-4 Suppresses Proliferation of A549 Cells. The mTOR pathway plays a key role in regulating many cellular processes, including cell metabolism, proliferation, apoptosis, and autophagy. It is not surprising, that the dysfunction of the mTOR kinase could promote aberrant survival or proliferation of cells.[42] Now that C-4 is a potential mTOR inhibitor, next we detect its effects on the growth of A549 cells. As shown in Figure 7A, the proliferation of A549 cells is strongly inhibited by C-4, and the inhibitory effect is time- and dose-dependent. In our tests, the IC_{50} of C-4 at 24 h is calculated as 3.176 μM (Figure S4), and such a high inhibition activity against A549 cells proliferation is comparable with that of PP242. As reported, the 24 h viability of A549 cells treated with about 5 μM PP242 can be reduced to 50%.[43] Cell cycle distribution analysis shows that the titration of C-4 gets more and more A549 cells stalled at the S phase, and fewer cells are in the G2 phase (Figure 7B). Furthermore, according to the results detected by inverted microscopy, C-4 ultimately causes cell death in a dose-dependent manner (Figure 7C). It is reasonable to conclude, that by inhibiting mTOR activity, C-4 blocks A549 cell growth through delaying the S phase progression of the A549 cell cycle and inducing cell death.

C-4 Induces Autophagy in A549 Cells. As a central factor in regulating autophagy initiation, mTOR fails to inhibit autophagy due to the weak sense of ATP caused by C-4 treatment, regardless of nutrients and energy context in the cell.[42,44,45] By using TEM, we find that A549 cells treated with 3.6 μg/mL C-4 display quite a number of autophagosomes in the cytoplasm. In part of the double-membrane bound APs, some undigested organelles and aggregated protein puncta can be obviously observed (Figure 8A,B). The autophagic puncta are also detected by confocal laser scanning microscopy. In Figure 8C,D, C4-treated A549 cells containing GFP-LC3 plasmids have LC3 puncta accumulated in the cytoplasm, indicating the occurrence of autophagic flux in the presence of C-4.

Besides, the expression level changes of key elements involved in the autophagic flux fit well with that of autophagy as well. As detected in A549 cells, the presence of C-4 induces remarkable upregulation of Beclin1, lipidation of LC3 (switching from LC3-I to LC3-II), and degradation of P62/SQSTM1 in a dose-dependent manner (Figure 9A). We also reveal that C-4 greatly upregulates the activity of a well-known autophagy initiator ULK1 by an increasing level of p-ULK1 (phosphorylated ULK1). To be specific, C-4 treatment induced upregulation of p-ULK1^{ser555} and downregulation of p-ULK1^{ser757}, with a total ULK1 expression exhibiting no apparent changes (Figure 9B). Consequently, autophagy in A549 cells can be activated by C-4 via inhibiting the mTOR kinase.[41,46,47] Considering increasing evidence for cell death by sustained autophagy,[48−50] the autophagy in A549 cells may contribute to the suppression of cell growth under C-4 treatment.

CONCLUSION

To conclude, we have developed a new mTOR pathway inhibitor through the integrated use of multilayer virtual screening and biological tests. As revealed, the newfound C-4 exhibits comparable inhibitory effects with that of PP242, and causes similar phenotypes to PP242 in A549 cells. C-4 is consequently supposed to block the mTOR pathway by inhibiting mTORC1 and mTORC2 simultaneously. Specifically, C-4 is regarded as a potential ATP-competitive mTOR inhibitor. It deprives both mTOR complexes of the ability to phosphorylate corresponding substrates by competing with ATP at the mTOR kinase site. Moreover, via inhibiting the mTOR pathway more comprehensively, A549 cells exposed to C-4 exhibit growth arrest, death, and autophagy, suggesting the potential of C-4 to be developed for anticancer therapies. Our success in discovering the mTOR inhibitor demonstrates that in silico approaches promote the drug discovery.

ASSOCIATED CONTENT

Supporting Information

The Supporting Information is available free of charge on the ACS Publications website at DOI: 10.1021/acs.molpharmaceut.8b00996.

Supplements to the description of pharmacophore model used for prospective virtual screening, supporting figures, and tables (PDF)

^{1}H NMR spectra and LC−MS spectra (PDF)

AUTHOR INFORMATION

Corresponding Authors

*E-mail: znchen@fmmu.edu.cn.

*E-mail: hzhang@fmmu.edu.cn.

ORCID

Jiyuan Liu: 0000-0002-3524-2064

Hai Zhang: 0000-0002-7999-0208

Author Contributions

J.Y.L, L.L., and Z.T. contributed equally to this work. J.Y.L. and H.Z. conceived the project. J.Y.L. and H.Z. designed the experiment. J.Y.L., L.L., T.Z., Y.F.L., C.H.S., J.L.S., S.H.W., Y.Z., C.Q.Z., and B.B. performed the experiments and prepared the manuscript. H.Z. and Z.N.C. supervised the study and contributed reagents/materials. All authors contributed to data analysis.

DOI: 10.1021/acs.molpharmaceut.8b00996
Mol. Pharmaceutics 2018, 15, 5427−5436

Notes

The authors declare no competing financial interest.

■ ACKNOWLEDGMENTS

The research was supported by the National Natural Science Foundation of China (Grant 21503272), the Fundamental Research Funds for the Central Universities (Grant 2452018008), and the General Financial Grant from the China Postdoctoral Science Foundation (Grant 2015M572753).

■ REFERENCES

(1) Zoncu, R.; Efeyan, A.; Sabatini, D. M. mTOR: from growth signal integration to cancer, diabetes and ageing. *Nat. Rev. Mol. Cell Biol.* **2011**, *12*, 21−35.
(2) Saxton, R. A.; Sabatini, D. M. mTOR signaling in growth, metabolism, and disease. *Cell* **2017**, *168*, 960−976.
(3) González, A.; Hall, M. N. Nutrient sensing and TOR signaling in yeast and mammals. *EMBO J.* **2017**, *36*, 397−408.
(4) Keith, C. T.; Schreiber, S. L. PIK-related kinases: DNA repair, recombination, and cell cycle checkpoints. *Science* **1995**, *270*, 50−51.
(5) Yang, H.; Rudge, D. G.; Koos, J. D.; Vaidialingam, B.; Yang, H. J.; Pavletich, N. P. mTOR kinase structure, mechanism and regulation. *Nature* **2013**, *497*, 217−223.
(6) Jung, C. H.; Ro, S. H.; Cao, J.; Otto, N. M.; Kim, D. H. mTOR regulation of autophagy. *FEBS Lett.* **2010**, *584*, 1287−1295.
(7) Dunlop, E.; Tee, A. mTOR and autophagy: a dynamic relationship governed by nutrients and energy. *Semin. Cell Dev. Biol.* **2014**, *36*, 121−129.
(8) Feldman, M. E.; Apsel, B.; Uotila, A.; Loewith, R.; Knight, Z. A.; Ruggero, D.; Shokat, K. M. Active-site inhibitors of mTOR target rapamycin-resistant outputs of mTORC1 and mTORC2. *PLoS Biol.* **2009**, *7*, e1000038.
(9) Sarbassov, D. D.; Guertin, D. A.; Ali, S. M.; Sabatini, D. M. Phosphorylation and regulation of Akt/PKB by the rictor-mTOR complex. *Science* **2005**, *307*, 1098−1101.
(10) Mammucari, C.; Milan, G.; Romanello, V.; Masiero, E.; Rudolf, R.; Del Piccolo, P.; Burden, S. J.; Di Lisi, R.; Sandri, C.; Zhao, J.; et al. FoxO3 controls autophagy in skeletal muscle in vivo. *Cell Metab.* **2007**, *6*, 458−471.
(11) Chen, S.; Han, Q.; Wang, X.; Yang, M.; Zhang, Z.; Li, P.; Chen, A.; Hu, C.; Li, S. IBP-mediated suppression of autophagy promotes growth and metastasis of breast cancer cells *via* activating mTORC2/Akt/FOXO3a signaling pathway. *Cell Death Dis.* **2013**, *4*, e842.
(12) Martelli, A. M.; Buontempo, F.; McCubrey, J. A. Drug discovery targeting the mTOR pathway. *Clin. Sci.* **2018**, *132*, 543−568.
(13) Kim, L. C.; Cook, R. S.; Chen, J. mTORC1 and mTORC2 in cancer and the tumor microenvironment. *Oncogene* **2017**, *36*, 2191−2201.
(14) Grunt, T. W.; Mariani, G. L. Novel approaches for molecular targeted therapy of breast cancer: interfering with PI3K/AKT/mTOR signaling. *Curr. Cancer Drug Targets* **2013**, *13*, 188−204.
(15) Thiyagarajan, V.; Lee, K.-W.; Leong, M. K.; Weng, C.-F. Potential natural mTOR inhibitors screened by *in silico* approach and suppress hepatic stellate cells activation. *J. Biomol. Struct. Dyn.* **2017**, 1−15.
(16) Khanfar, M. A.; AbuKhader, M. M.; Alqtaishat, S.; Taha, M. O. Pharmacophore modeling, homology modeling, and *in silico* screening reveal mammalian target of rapamycin inhibitory activities for sotalol, glyburide, metipranolol, sulfamethizole, glipizide, and pioglitazone. *J. Mol. Graphics Modell.* **2013**, *42*, 39−49.
(17) Wander, S. A.; Hennessy, B. T.; Slingerland, J. M. Next-generation mTOR inhibitors in clinical oncology: how pathway complexity informs therapeutic strategy. *J. Clin. Invest.* **2011**, *121*, 1231−1241.
(18) Benjamin, D.; Colombi, M.; Moroni, C.; Hall, M. N. Rapamycin passes the torch: a new generation of mTOR inhibitors. *Nat. Rev. Drug Discovery* **2011**, *10*, 868−880.
(19) Liu, J. Y.; Chen, X. E.; Zhang, Y. L. Insights into the key interactions between human protein phosphatase 5 and cantharidin using molecular dynamics and site-directed mutagenesis bioassays. *Sci. Rep.* **2015**, *5*, 12359.
(20) Tian, Z.; Liu, J.; Zhang, Y. Structural insights into *Cydia pomonella* pheromone binding protein 2 mediated prediction of potentially active semiochemicals. *Sci. Rep.* **2016**, *6*, 22336.
(21) Liu, J.; Tian, Z.; Zhang, Y. Structure-based discovery of potentially active semiochemicals for *Cydia pomonella* (L.). *Sci. Rep.* **2016**, *6*, 34600.
(22) Wang, J.; Wolf, R. M.; Caldwell, J. W.; Kollman, P. A.; Case, D. A. Development and testing of a general amber force field. *J. Comput. Chem.* **2004**, *25*, 1157−1174.
(23) Jakalian, A.; Jack, D. B.; Bayly, C. I. Fast, efficient generation of high-quality atomic charges. AM1-BCC model: II. Parameterization and validation. *J. Comput. Chem.* **2002**, *23*, 1623−1641.
(24) Hummer, G.; Rasaiah, J. C.; Noworyta, J. P. Water conduction through the hydrophobic channel of a carbon nanotube. *Nature* **2001**, *414*, 188−190.
(25) Berendsen, H. J.; Postma, J. V.; van Gunsteren, W. F.; DiNola, A.; Haak, J. Molecular dynamics with coupling to an external bath. *J. Chem. Phys.* **1984**, *81*, 3684−3690.
(26) Tian, Z.; Liu, J.; Zhang, Y. Key residues involved in the interaction between *Cydia pomonella* pheromone binding protein 1 (CpomPBP1) and Codlemone. *J. Agric. Food Chem.* **2016**, *64*, 7994−8001.
(27) Liu, J.; Tian, Z.; Zhou, N.; Liu, X.; Liao, C.; Lei, B.; Li, J.; Zhang, S.; Chen, H. Targeting the apoptotic Mcl-1-PUMA interface with a dual-acting compound. *Oncotarget* **2017**, *8*, 54236−54242.
(28) Miller, B. R., III; McGee, T. D., Jr; Swails, J. M.; Homeyer, N.; Gohlke, H.; Roitberg, A. E. MMPBSA. py: an efficient program for end-state free energy calculations. *J. Chem. Theory Comput.* **2012**, *8*, 3314−3321.
(29) Kollman, P. A.; Massova, I.; Reyes, C.; Kuhn, B.; Huo, S.; Chong, L.; Lee, M.; Lee, T.; Duan, Y.; Wang, W.; et al. Calculating structures and free energies of complex molecules: combining molecular mechanics and continuum models. *Acc. Chem. Res.* **2000**, *33*, 889−897.
(30) Hou, T.; Wang, J.; Li, Y.; Wang, W. Assessing the performance of the MM/PBSA and MM/GBSA methods. 1. The accuracy of binding free energy calculations based on molecular dynamics simulations. *J. Chem. Inf. Model.* **2011**, *51*, 69−82.
(31) Hou, T.; Wang, J.; Li, Y.; Wang, W. Assessing the performance of the molecular mechanics/Poisson Boltzmann surface area and molecular mechanics/generalized Born surface area methods. II. The accuracy of ranking poses generated from docking. *J. Comput. Chem.* **2011**, *32*, 866−877.
(32) Moreira, I. S.; Fernandes, P. A.; Ramos, M. J. Computational alanine scanning mutagenesis-an improved methodological approach. *J. Comput. Chem.* **2007**, *28*, 644−654.
(33) Wolber, G.; Langer, T. LigandScout: 3D pharmacophores derived from protein-bound ligands and their use as virtual screening filters. *J. Chem. Inf. Model.* **2005**, *45*, 160−169.
(34) Cavasotto, C. N.; Palomba, D. Expanding the horizons of G protein-coupled receptor structure-based ligand discovery and optimization using homology models. *Chem. Commun.* **2015**, *51*, 13576−13594.
(35) Kumar, G.; Agarwal, R.; Swaminathan, S. Discovery of a fluorene class of compounds as inhibitors of botulinum neurotoxin serotype E by virtual screening. *Chem. Commun.* **2012**, *48*, 2412−2414.
(36) Vinter, J. G. Extended electron distributions applied to the molecular mechanics of some intermolecular interactions. *J. Comput.-Aided Mol. Des.* **1994**, *8*, 653−668.
(37) Woods, C. J.; Malaisree, M.; Hannongbua, S.; Mulholland, A. J. A water-swap reaction coordinate for the calculation of absolute

DOI: 10.1021/acs.molpharmaceut.8b00996
Mol. Pharmaceutics 2018, 15, 5427−5436

protein-ligand binding free energies. *J. Chem. Phys.* **2011**, *134*, 054114.
(38) Woods, C. J.; Malaisree, M.; Michel, J.; Long, B.; McIntosh-Smith, S.; Mulholland, A. J. Rapid decomposition and visualisation of protein-ligand binding free energies by residue and by water. *Faraday Discuss.* **2014**, *169*, 477−499.
(39) Woods, C. J.; Malaisree, M.; Long, B.; McIntosh-Smith, S.; Mulholland, A. J. Computational assay of H7N9 influenza neuraminidase reveals R292K mutation reduces drug binding affinity. *Sci. Rep.* **2013**, *3*, 3561.
(40) Pons, J.; Rajpal, A.; Kirsch, J. F. Energetic analysis of an antigen/antibody interface: alanine scanning mutagenesis and double mutant cycles on the HyHEL-10/lysozyme interaction. *Protein Sci.* **1999**, *8*, 958−968.
(41) Rodrik-Outmezguine, V. S.; Okaniwa, M.; Yao, Z.; Novotny, C. J.; McWhirter, C.; Banaji, A.; Won, H.; Wong, W.; Berger, M.; de Stanchina, E.; et al. Overcoming mTOR resistance mutations with a new-generation mTOR inhibitor. *Nature* **2016**, *534*, 272−276.
(42) Jiang, X.; Overholtzer, M.; Thompson, C. B. Autophagy in cellular metabolism and cancer. *J. Clin. Invest.* **2015**, *125*, 47−54.
(43) Jin, H.; Hong, S.; Park, J.; Chang, Y.; Hong, Y.; Park, I.; Lee, J. Inhibition of JNK-mediated autophagy enhances NSCLC cell sensitivity to mTORC1/2 inhibitors. *Sci. Rep.* **2016**, *6*, 28945.
(44) Yu, L.; McPhee, C. K.; Zheng, L.; Mardones, G. A.; Rong, Y.; Peng, J.; Mi, N.; Zhao, Y.; Liu, Z.; Wan, F.; et al. Termination of autophagy and reformation of lysosomes regulated by mTOR. *Nature* **2010**, *465*, 942−946.
(45) Rong, Y.; McPhee, C. K.; Deng, S.; Huang, L.; Chen, L.; Liu, M.; Tracy, K.; Baehrecke, E. H.; Yu, L.; Lenardo, M. J. Spinster is required for autophagic lysosome reformation and mTOR reactivation following starvation. *Proc. Natl. Acad. Sci. U. S. A.* **2011**, *108*, 7826−7831.
(46) Zhang, L.; Fu, L.; Zhang, S.; Zhang, J.; Zhao, Y.; Zheng, Y.; He, G.; Yang, S.; Ouyang, L.; Liu, B. Discovery of a small molecule targeting ULK1-modulated cell death of triple negative breast cancer in vitro and in vivo. *Chem. Sci.* **2017**, *8*, 2687−2701.
(47) Wang, X.; Wei, S.; Zhao, Y.; Shi, C.; Liu, P.; Zhang, C.; Lei, Y.; Zhang, B.; Bai, B.; Huang, Y.; Zhang, H. Anti-proliferation of breast cancer cells with itraconazole: Hedgehog pathway inhibition induces apoptosis and autophagic cell death. *Cancer Lett.* **2017**, *385*, 128−136.
(48) Liu, J. J.; Lin, M.; Yu, J. Y.; Liu, B.; Bao, J. K. Targeting apoptotic and autophagic pathways for cancer therapeutics. *Cancer Lett.* **2011**, *300*, 105−114.
(49) Kroemer, G. Autophagy: a druggable process that is deregulated in aging and human disease. *J. Clin. Invest.* **2015**, *125*, 1−4.
(50) Ke, B.; Tian, M.; Li, J.; Liu, B.; He, G. Targeting programmed cell death using small-molecule compounds to improve potential cancer therapy. *Med. Res. Rev.* **2016**, *36*, 983−1035.

DOI: 10.1021/acs.molpharmaceut.8b00996
Mol. Pharmaceutics 2018, 15, 5427−5436